Nanophase-Separation in Immiscible Double-Network Elastomers Induces Synergetic Strengthening, Toughening, and Fatigue-Resistance

Journal:	*Chemistry of Materials*
Manuscript ID	cm-2021-00512z.R2
Manuscript Type:	Article
Date Submitted by the Author:	n/a
Complete List of Authors:	Zheng, Yong; Hokkaido University , Graduate School of Life Science Kiyama, Ryuji; Hokkaido University , Graduate School of Life Science Matsuda, Takahiro; Hokkaido University, Cui, Kunpeng; Hokkaido University Li, Xueyu; Hokkaido University Cui, Wei; Hokkaido University Guo, Yunzhou; Hokkaido University Nakajima, Tasuku; Hokkaido University , Faculty of Advanced Life Science Kurokawa, Takayuki; Hokkaido University, Gong, Jian Ping; Hokkaido University , Faculty of Advanced Life Science

Nanophase-Separation in Immiscible Double-Network Elastomers Induces Synergetic Strengthening, Toughening, and Fatigue-Resistance

Yong Zheng[1], Ryuji Kiyama[1], Takahiro Matsuda[2], Kunpeng Cui[3], Xueyu Li[4], Wei Cui[4], Yunzhou Guo[1], Tasuku Nakajima[2,3,4]*, Takayuki Kurokawa[2,4], and Jian Ping Gong[2,3,4]*

[1]*Graduate School of Life Science, Hokkaido University, Sapporo 001-0021, Japan*

[2]*Faculty of Advanced Life Science, Hokkaido University, Sapporo 001-0021, Japan*

[3]*Institute for Chemical Reaction Design and Discovery (WPI-ICReDD), Hokkaido University, Sapporo 001-0021, Japan*

[4]*Global Station for Soft Matter, Global Institution for Collaborative Research and Education (GI-CoRE), Hokkaido University, Sapporo 001-0021, Japan*

*Corresponding authors: tasuku@sci.hokudai.ac.jp; gong@sci.hokudai.ac.jp

ABSTRACT

High modulus, toughness, and fatigue-resistance are usually difficult to be obtained simultaneously in rubbery materials. Here, we report that by superimposing nanophase-separation structure in double-network elastomers using immiscible polymers, the modulus, fracture energy, and energy release rate of fatigue threshold are enhanced all together by 13, 5, and 5 times, respectively. We reveal that the interplay between the double-network structure and the nanophase-separation structure brings two effects synergistically: (1) formation of nanoclusters overstresses and homogenizes the sacrificial network, thereby remarkably increasing the modulus and yielding stress; (2) the nanoclusters act as viscoelastic nanofillers dissipating energy and pinning the crack propagation, thereby significantly enhancing toughness and fatigue-resistance. This work provides a facile approach to superimpose high-order structures in double-network materials for excellent mechanical performance. The clarified synergetic effects should be universal for double-network materials made of immiscible polymers. We believe that this work will facilitate more studies on elastomers and gels along this line.

INTRODUCTION

Rubbery materials, featured by softness and stretchability, are extensively used as structural materials in many fields where load-bearing and shock-absorbing abilities are required.[1–3] Improving the mechanical performance of rubbery materials, including modulus, strength, toughness and fatigue resistance, is one of the major subjects for their further wide applications. Specifically, high modulus and high strength bring better load-bearing ability while high toughness and fatigue resistance directly impact safety and service lifetime of the materials. These mechanical properties are difficult to be improved simultaneously. For example, increasing modulus usually results in a sacrifice of the deformability and toughness of material. Recent studies have shown that employing molecular-energy-dissipation mechanisms by sacrificial bonds, either covalent or noncovalent, effectively enhances both the mechanical strength and toughness of soft materials.[4–16] However, the fatigue resistance is hardly improved by energy-dissipation of covalent or noncovalent sacrificial bonds.[17, 18]

In this work, we report that formation of nanophase-separation structure in double-network (DN) elastomers significantly enhances the elastic modulus, strength, fracture toughness, and fatigue resistance all together in comparison to the mere DN elastomers. The contrasting network structure required for a DN material and the nanoscale phase separation are achieved simultaneously by using ionic polymer as the first network and non-polar polymer as the second network.[19] Specifically, a polyelectrolyte network is first prepared and then immersed in a precursor solution of the second network using a

cosolvent of high dielectric constant.[6, 19] The first polyelectrolyte network swells considerably in the second precursor solution owing to the high osmotic pressure originating from dissociated counterions, thereby making the network prestretched and brittle. Then, the stretchable second network is formed in the brittle first one, producing DN gels showing a highly contrasting architecture. Finally, the cosolvent in the DN gels is removed to obtain DN elastomers. Owing to the interpenetrated network structure of the double network materials, phase separation of these two immiscible polymers is pinned at nanoscale in the DN elastomers. As a result, DN elastomers with nanophase-separation structure are formed.

To control the nanophase-separation, we use copolymer made from ionic and non-polar monomers as the first network and homopolymer made from non-polar monomers as the second. We systematically tune the nanophase separation by changing the ionic-monomer fraction in the first network while maintaining almost the same primary double-network structure. The nanophase-separation structure in the DN elastomers is clarified by small-angle X-ray scattering (SAXS) and transmission electron microscopy (TEM). We next investigate the effects of the nanophase-separated structure on the internal fracture and energy dissipation during tensile deformation in DN elastomers. The effect of the nanophase-separated structure on the fracture and fatigue resistance of the DN elastomers is also studied. We elucidate that the interplay mechanism between the double network structure and the nanophase separation structure enhances the elastic modulus, strength, fracture toughness, and fatigue resistance all together. This work provides a facile approach to superimpose high-order structures in double

network materials for excellent mechanical performance. The clarified synergetic effect should be universal for double network materials made of immiscible polymers. We believe that this work will facilitate more studies on elastomers and gels along this line.

RESULTS AND DISCUSSION

Fabrication of DN Elastomers with Tuned Nanophase Separation. The chemical structures of the monomers and solvent are shown in Figure 1A. Our DN elastomers were fabricated through the same sequential free-radical polymerization as that used to prepare DN gels, as shown in Figure 1B. First, a highly crosslinked copolymer network poly(MEA-*co*-AMPS) was synthesized from an *N*-methylformamide (NMF) solution containing the ionic monomer 2-acrylamido-2-methylpropanesulfonic acid (AMPS) and the non-polar monomer 2-methoxyethyl acrylate (MEA) with the prescribed AMPS molar fraction (f_{AMPS}), cross-linker, and initiator. The as-prepared copolymer network P(MEA-*co*-AMPS) is referred to as "the first single network", S_1N-f_{AMPS}. All the S_1N-f_{AMPS} gels with NMF solvent were transparent without macroscopic phase separation. Then, the S_1N-f_{AMPS} gels were immersed in the second-network precursor solution containing the non-polar monomer MEA, cross-linker, and initiator in the polar solvent NMF (40 weight % (wt %)). A small amount of f_{AMPS} could bring substantial swelling of the copolymer gels in the second-network precursor solution, owing to the osmotic pressure of the dissociated counterions in the gels.[19] Figure S1 shows the swollen S_1N-0 and S_1N-0.1 gels, demonstrating that using as little as 10 mol% of the ionic monomer in the copolymerization could considerably swell the S_1N, thereby effectively prestretching the first-network strands. After the second polymerization, the non-polar PMEA network (hereinafter referred to as S_2N) interpenetrating with the first network was formed. The as-synthesized DN gels containing NMF as solvent are hereafter

referred to as DN-f_{AMPS} gels. The DN elastomers were obtained by removing NMF from the precursor DN gels. All the DN elastomers are highly transparent regardless of the f_{AMPS}, as shown in Figure 1D and Figure S1B, indicating that macroscopic phase separation was suppressed by the interpenetrated double-network structure even for DN elastomers with high f_{AMPS}.

Here, we denote the prestretch ratios of the swollen first network relative to those of its corresponding as-synthesized gel as $\lambda_{s,g}$ and $\lambda_{s,el}$ for the DN gels and DN elastomers, respectively, as illustrated in Figure 1B, where $\lambda_{s,g}$ and $\lambda_{s,el}$ represent the ratios of the DN gel and elastomer thicknesses to those of their corresponding as-synthesized S_1N gels, respectively. Figure 1C presents $\lambda_{s,g}$, $\lambda_{s,el}$, and the corresponding volume fraction of the first network (φ_{1st}) in the DN elastomers as functions of f_{AMPS}. For $f_{AMPS} = 0$, owing to the low swelling ability of the S_1N-0 gel, the prestretch ratios $\lambda_{s,g}$ and $\lambda_{s,el}$ are small ($\lambda_{s,g} \approx 1.25$ and $\lambda_{s,el} \approx 1.10$), and the corresponding volume fraction of the first network (φ_{1st}) in the DN-0 elastomer is as high as 20.4%. For $f_{AMPS} \geq 0.1$, owing to the substantial increase in the swelling ability of the S_1N gel, the prestretch ratios ($\lambda_{s,g} \geq 2.00$ and $\lambda_{s,el} \geq 1.70$) increased, and the volume fraction of the first network ($\varphi_{1st} < 5\%$) decreased remarkably. These results indicate that for $f_{AMPS} \geq 0.1$, a contrasting double-network structure is formed in the DN gels and DN elastomers. Because $\lambda_{s,g}$, $\lambda_{s,el}$, and φ_{1st} are almost identical for $f_{AMPS} \geq 0.1$, the primary double-network structure in these DN gels and DN elastomers should be almost identical.

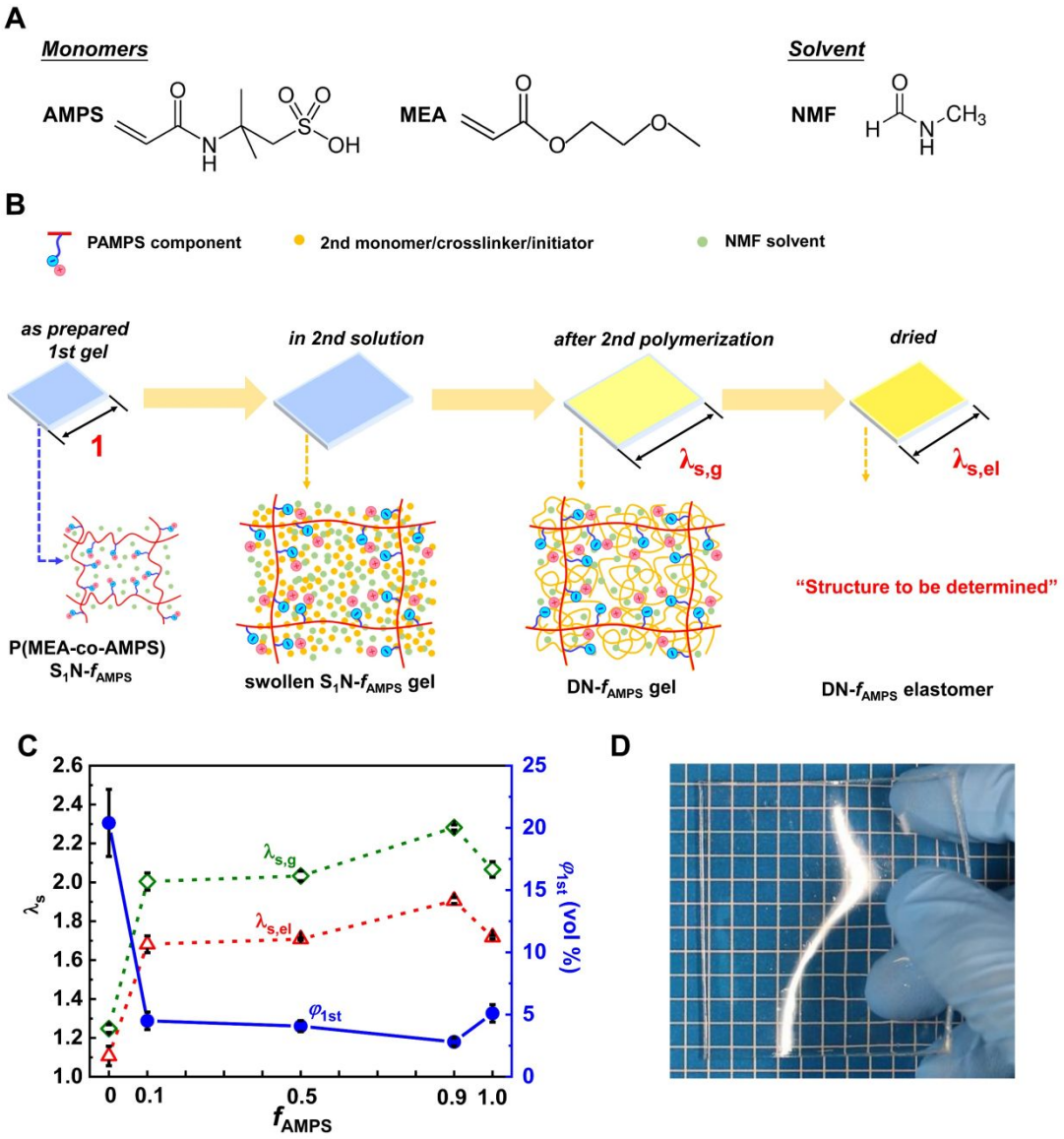

Figure. 1. Preparation of immiscible DN elastomers. (A) Chemical structure of monomers and solvent. (B) Schematic illustrating fabrication of P(MEA-*co*-AMPS)/PMEA DN elastomers. (C) Prestretch ratios (λ_s) of swollen first networks relative to as-prepared ones ($\lambda_{s,g}$ for DN gel and $\lambda_{s,el}$ for DN elastomer) and volume fraction of first network (φ_{1st}) in DN elastomers plotted as functions of AMPS molar fraction in first network (f_{AMPS}). (D) Digital photo of DN-1.0 elastomer.

Nanophase Separation Structure. We next conducted synchrotron radiation small-angle X-ray scattering (SAXS) measurements to investigate the nanophase-separated structure in the DN elastomers. SAXS measurements, wherein q ranges from 0.027 to 0.70 nm^{-1}, can capture structural lengths from 9 to 233 nm. Here, $q = 4\pi\sin\theta/\lambda$ is the modulus of the scattering vector, 2θ is the scattering angle, and λ is the X-ray

wavelength. For the samples prepared with $f_{AMPS} < 0.4$, no scattering ring is present in the 2D SAXS patterns (Figure 2A), and no correlation peak arises in the 1D scattering intensity profiles (Figure 2B), indicating the absence of any phase-separated structure in the observed length range. In contrast, for the samples prepared with $f_{AMPS} \geq 0.4$, a circular scattering ring appears (Figure 2A) and a broad correlation peak (q_{peak}) at ~0.14 nm^{-1} in the 1D scattering-intensity profiles (Figure 2B) are observed, indicating nanostructure formation in the DN elastomers. As the hydrophilic PAMPS and hydrophobic PMEA phases are poorly miscible, the inclusion of an S_1N network in the hydrophobic S_2N polymer matrix when $f_{AMPS} \geq 0.4$ (despite a very low φ_{1st}) results in ionic cluster formation through dipole-dipole interaction, thus causing nanophases separation in the DN elastomers. For comparison, we also conducted SAXS measurements on DN gels. Regardless of f_{AMPS}, all the DN gels show no scattering ring in the 2D SAXS patterns and no correlation peak in the 1D scattering-intensity profiles, demonstrating the absence of the phase-separated structure (Figure S2). These results indicate that the phase-separated structure in DN elastomers is formed during the drying of the DN gels.

The peak position (q_{peak}) in Figure 2B corresponds to a characteristic structural length (*d*-spacing between adjacent ionic clusters) d_0 of ~45 nm according to the equation $d_0 = 2\pi/q_{peak}$, which is much shorter than the wavelength of visible light and thus accounts for the high transparency of the DN elastomers. The scattered intensities of the rings in the 2D patterns (Figure 2A) and the corresponding correlation peaks in the 1D profiles (Figure 2B) increased with increasing f_{AMPS} for $f_{AMPS} \geq 0.4$, suggesting that the phase contrast or volume of ionic clusters increases with increasing f_{AMPS}, while d_0 hardly changes with increasing f_{AMPS} in the range of 40–45 nm, as illustrated in Figure 2C. In addition, $FWHM/q_{peak}$ remained constant with increasing f_{AMPS} (Figure

S3), indicating that the distribution of ionic clusters in the DN elastomers is independent of f_{AMPS}, where *FWHM* is the full width at half maximum of the correlation peak in the 1D profiles.[20, 21] The above SAXS results show that (1) the obvious ionic cluster structure arises at $f_{AMPS} \geq 0.4$; (2) the average intercluster distance (d_0) is approximately 40–45 nm; and (3) the distribution of the ionic clusters is independent of f_{AMPS}. Such nanophase-separation structure is similar to those found in ionomers such as sulfonated and quaternary-ammonium-functionalized block copolymers [22–25].

To further verify the structural pictures deduced from the SAXS results, we conducted transmission electron microscopy (TEM) on the Cs^+-stained DN-1.0 elastomer (see Materials and Methods). Cs^+ ions selectively stain PAMPS sulfonate ions. The TEM image shown in Figure 2D reveals an island-sea structure. The dark irregularly shaped islands should be assigned to the PAMPS-rich phase that is densely stained by Cs^+, while the bright sea phase should be assigned to the PAMPS-poor phase. We confirmed that the phase separation does not cause permanent damage to the materials (Figure S4), meaning that the two networks maintain the bicontinuous structure even after phase separation. Thereby, the PAMPS strands are collapsed in the PAMPS-rich islands and are overstretched in the PAMPS-poor sea owing to the mass transfer of the loosely crosslinked second-network PMEA from the island phase to the sea phase. The average distance (*d*) between the dark islands is on the order of tens of nanometers, which is in accordance with the SAXS results.

To clarify whether a PAMPS-rich cluster contains multiple first-network strands, we compared the average size of a dark island in the TEM image with the average mesh size (ξ_{el}) of the first network strands in the DN elastomer. We first estimate the mesh size or the end-to-end distance (ξ_0) of the first network strands at Gaussian conformation from the shear modulus (μ) of the as-prepared S_1N gel using $\mu = \frac{k_B T}{{\xi_0}^3}$,

where k_B and T are the Boltzmann constant and absolute temperature, respectively[26, 27]. For the S_1N-1.0 gel, $\mu = 3.0 \times 10^4$ Pa from rheology measurement at $T = 298$ K, and we have $\xi_0 = 5.1$ nm. The first network in the DN elastomer is swollen compared to the as-prepared S_1N gel by a factor of $\lambda_{s,el} = 1.7$ on average. Therefore, the average mesh size of the first network in the DN-1.0 elastomer (ξ_{el}) ≈ 8.7 nm, which is much smaller than the average diameter of the dark islands (~ 30 nm). As the first-network strands are collapsed in the PAMPS-rich phase and its size is smaller than ξ_{el}, we conclude that each PAMPS-rich island contains multiple collapsed first-network strands.

Next, we discuss the structure in the PAMPS-poor phase. We compared the distance between PAMPS-rich clusters with the average length of a fully stretched first-network strand (L_c). For DN gels, our previous studies have shown that the yielding stretch ratio is related to the maximum stretch ratio of the first-network strands, $\lambda_y\lambda_{s,g} \approx L_c/R_0$, where R_0 is the average end-to-end distance of the as-prepared first-network strands [28, 29]. For the DN-1.0 gel, $\lambda_y\lambda_{s,g} \approx 6$ (see later text and Figure S6), and $R_0 \approx \xi_0$, hence $L_c \approx 31$ nm. The contour length (L_c) of the first-network strands is approximately the intercluster distance of the PAMPS-rich phases (~ 40 nm). Therefore, we conclude that only single or few network strands exist between the PAMPS-rich phases and that the PAMPS-rich phases are hyperconnected by these overstretched first-network strands. We assume that the nanophase separation should effectively homogenize the first network structure in the PAMPS-poor phase since the tension applied on each strand is automatically adjusted by the phase separation. We confirmed that all the DN elastomers show the same glass-transition temperature ($T_g \approx -35$ °C), which corresponds to the glass transition of the non-polar PMEA, while no clear PAMPS-related T_g was observed in the DSC thermograms (Figure S5), suggesting that

the PAMPS-rich phases are in a viscoelastic state with abundant dynamic dipole-dipole interaction, similar to those in ionomers.[30]

From the foregoing analysis, we schematically illustrate the super-double-network structure of the immiscible-polymer-based DN elastomers in Figure 2E. For high f_{AMPS} ($\geq$ 0.4), the first-network strands collapse, forming PAMPS-rich nanoclusters and PAMPS-poor phase in the surrounding region. As the elastomers are almost incompressible, the second network is squeezed from the PAMPS-rich clusters, thereby increasing the second-network volume ratio in the PAMPS-poor region, which stretches the first-network strands in this phase. Consequently, nanophase separation enhances the contrasting double-network structure in the PAMPS-poor phase.

The size of the PAMPS-rich clusters should be determined by the balance between the free energy of demixing of the two immiscible polymers that drives the phase separation and the free energy of elasticity of the network that restricts the phase separation. The overstretched first network in the PAMPS-poor phase should contribute predominantly to the free energy of elasticity that restricts the phase separation.

For low f_{AMPS} (< 0.4), no obvious phase separation occurs (Figure 2C), and the first-network strands are modestly and homogenously prestretched in these DN elastomers, showing a slightly lower prestretch ratio (by a factor of $\lambda_{s,el}/\lambda_{s,g}$) than their corresponding DN gels (Figure 1C).

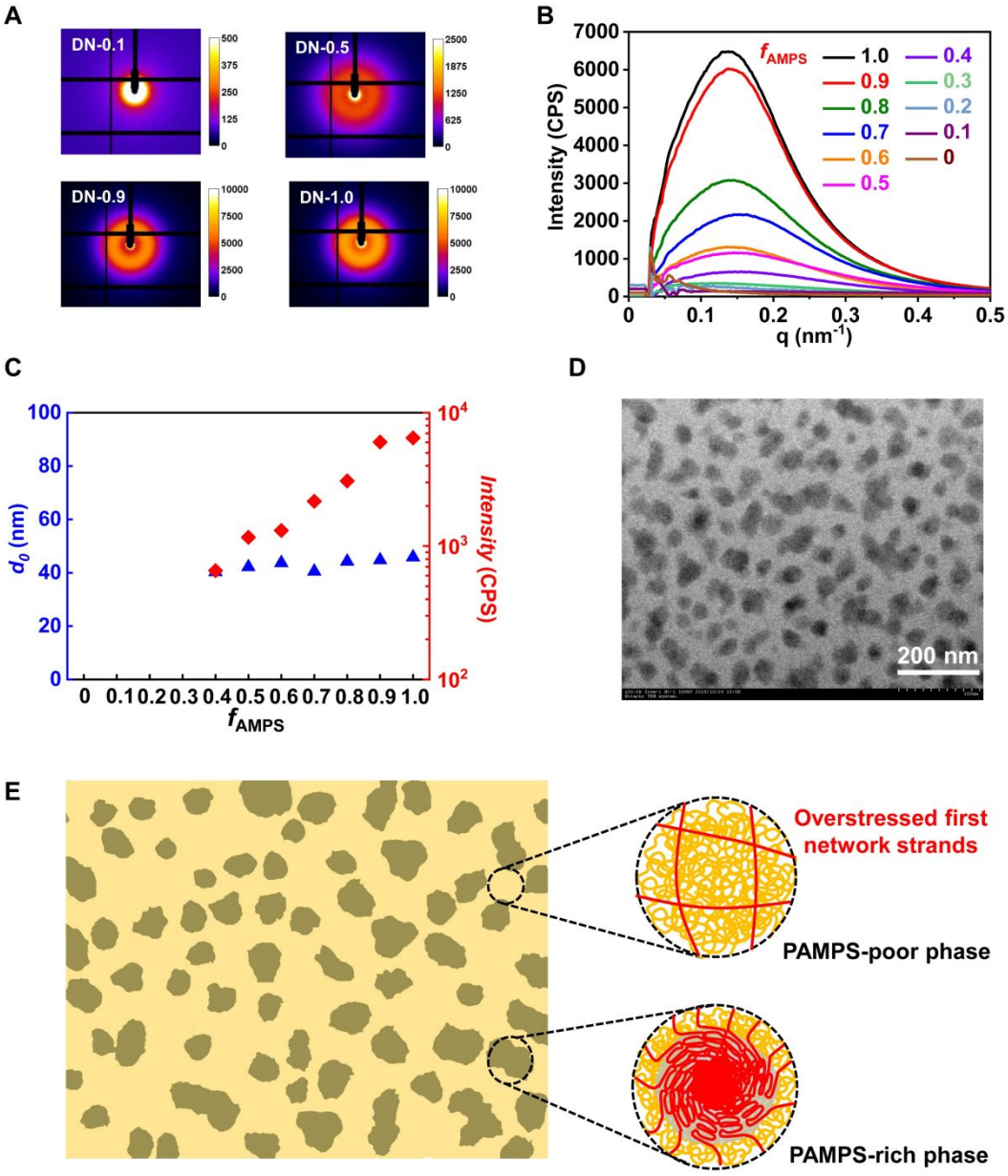

Figure 2. Characterization of nano-clustered structures in DN-f_{AMPS} elastomers. (A) Representative 2D SAXS patterns and (B) 1D scattering intensity profiles of DN elastomers prepared with various f_{AMPS} molar ratios. (C) *d*-spacing (d_0) and peak intensity plotted as functions of f_{AMPS} molar ratio, as obtained from (B). (D) Cs^+-stained TEM image of DN-1.0 elastomer. Dark and light regions correspond to PAMPS-rich and -poor phases, respectively. (E) Schematic illustrating DN-f_{AMPS} elastomer structures prepared with nanophase separation ($f_{AMPS} \geq 0.4$). With phase-separation, volume fractions of PAMPS in PAMPS-rich and -poor phases are much higher and lower than average value (φ_{1st}), respectively, and PAMPS strands are collapsed and overstretched in PAMPS-rich and -poor phases, respectively. Consequently, PAMPS-rich phase shows dynamic dipole-dipole interaction and serves as viscoelastic nanofillers, and PAMPS-poor phase shows enhanced contrasting double-network structure compared with counterpart elastomer structures prepared without phase separation.

Tensile Behaviors. To elucidate the effect of the nanophase-separated structure on the mechanical behavior of the DN elastomers, we compared the uniaxial tensile behaviors of the DN elastomers and their corresponding DN gels at a strain rate 0.14 s^{-1}. The results are shown in Figure 3. For $f_{AMPS} \geq 0.1$, the DN gels show marginal yielding, a phenomenon characteristic of typical DN hydrogels[31], while the DN gel prepared with $f_{AMPS} = 0$ does not show this feature. These results confirm that the DN gels prepared with $f_{AMPS} \geq 0.1$ have a contrasting network structure required for the double-network effect. Surprisingly, for $f_{AMPS} \geq 0.1$, the DN elastomers show distinct yielding and remarkable necking, with substantially increased stretch ratios at break, while the DN elastomer prepared with $f_{AMPS} = 0$ does not.

Furthermore, as seen in Figure 3A, B, although the mechanical behaviors of DN gels and DN elastomers are enhanced with increasing f_{AMPS}, they are more enhanced in DN elastomers than in the corresponding DN gels. We notice that all the DN elastomers show substantially increased stretch ratios at break comparing with the corresponding DN gels. This implies that the chain friction between the two networks play a role in force transfer and the enhanced chain friction in the solvent-free DN elastomers favors the load transfer from the second network to the first network.[32]

All the tensile properties of DN elastomers and DN gels are also summarized in Table. S1. For example, Young's modulus E, yielding stress σ_y, and work of extension W_b of the DN-1.0 elastomer is 13, 3, and 2.3 times higher than those of the DN-0.1elastomer, respectively, even though the volume fraction of first network φ_{1st} is almost the same for the two elastomers, indicating that the phase-separation induced significant improvement of the mechanical properties.

As revealed in previous studies, owing to the highly contrasting structure, the mechanical behavior of a DN gel and a multiple-network elastomer is dominated by the

first network that is in highly prestretched state before yielding.[28, 33, 34] Accordingly, to quantitatively compare the mechanical behavior of a DN elastomer with that of its corresponding DN gel, we need to normalize the strand density and prestretch level of the first network in both systems. Here, we adopt the as-synthesized first network (S_1N gel) as the reference state and rescale the nominal stress (σ) and stretch ratio (λ) by the prestretch ratio (λ_s) as $\sigma\lambda_s^2$ and $\lambda\lambda_s$, respectively[28, 33], where λ_s has been defined in Figure 1B. Figure 3C shows the rescaled stress-stretch ratio curves for DN gels and DN elastomers prepared with various f_{AMPS}. For $f_{AMPS} = 0$, the DN-elastomer curve exactly overlaps with that of the corresponding DN-gel. Overlapping of the stress-stretch curves is also observed for DN elastomer and DN gel of $f_{AMPS} = 0.1$ that show distinct yielding and remarkable necking. Whereas for $f_{AMPS} \geq 0.5$, the DN-elastomer curves deviate largely from those of DN-gels, and the deviation increases with increasing f_{AMPS}. This means that for $f_{AMPS} = 0$ or 0.1, the deformation behaviors of the DN elastomers and DN gels are only determined by the strand density and prestretch ratio of the first network, while for $f_{AMPS} \geq 0.5$, different mechanisms control the mechanical behavior of the DN elastomer. These results are consistent with the observation that a nanophase-separated structure is formed in DN elastomers when $f_{AMPS} \geq 0.4$ and clearly show that the nanophase-separated structure accounts for the significantly improved mechanical behavior of DN elastomers.

Figure 3D, E and Figure S5 show the rescaled Young's modulus ($E\lambda_s$), yielding stress ($\sigma_y\lambda_s^2$), and yielding stretch ratio ($\lambda_y\lambda_s$) extracted from Figure 3C**,** plotted as functions of f_{AMPS}. For the DN gels, $E\lambda_s$ is almost independent of f_{AMPS}, while $\sigma_y\lambda_s^2$ slightly increases and $\lambda_y\lambda_s$ slightly decreases with increasing f_{AMPS}. These results are consistent with the prediction that the primary double-network structure produced for different f_{AMPS} is almost identical in these DN gels, as suggested by Figure 1C. In

contrast, DN elastomers show strong f_{AMPS} dependence, especially for high f_{AMPS} at which the nanophase-separated structure is formed. Accordingly, we divided the figures according to regimes I and II wherein DN elastomers did not show any phase separation and showed obvious nanophase separation, respectively. Clearly, in regime I, the rescaled modulus $E\lambda_s$, yielding stress $\sigma_y{\lambda_s}^2$ and yielding stretch ratio $\lambda_y\lambda_s$ of all the DN elastomers are almost identical to those of the corresponding DN gels. Contrastingly, in regime II, the rescaled modulus ($E\lambda_s$) of the DN gels remain almost constant at ~0.2 MPa, independent of f_{AMPS}, while those of the corresponding DN elastomers remarkably increase with increasing f_{AMPS}. For the DN elastomer f_{AMPS} = 1.0, the rescaled modulus reaches 3.0 MPa, more than 10 times higher than that of the corresponding DN gel. We consider that the remarkable increase of modulus of DN elastomers with strong nanophase-separated structures is from the contribution of the overstressed first-network strands in the PAMPS-poor phase.

The rescaled $\sigma_y{\lambda_s}^2$ modestly increases, while the rescaled $\lambda_y\lambda_s$ only slightly decreases with increasing f_{AMPS} for the DN elastomers, as shown in Figure 3E and Figure S6, respectively. The difference between $\sigma_y{\lambda_s}^2$ for the DN elastomers and DN gels becomes large for high f_{AMPS} in regime II. As revealed by a previous study, the yielding of DN hydrogels corresponds to the first network rupturing into discontinuous fragments, and the yielding stress is proportional to the areal density of the load-bearing first-network strands, while the yielding stretch ratio corresponds to the average stretching limit of the first-network strands.[28] According to this molecular mechanism, at the yielding point, the areal density of the load bearing first-network strands in the strongly phase-separated DN elastomers is higher than that of the corresponding DN gels when compared at the same reference state. Although the strands in the PAMPS-poor phases are overstressed owing to strong phase separation, the rescaled $\lambda_y\lambda_s$ is

only slightly decreased, which suggests unfolding of the collapsed PAMPS strands in the PAMPS-rich phases under stretching by breaking of dipole-dipole interaction.

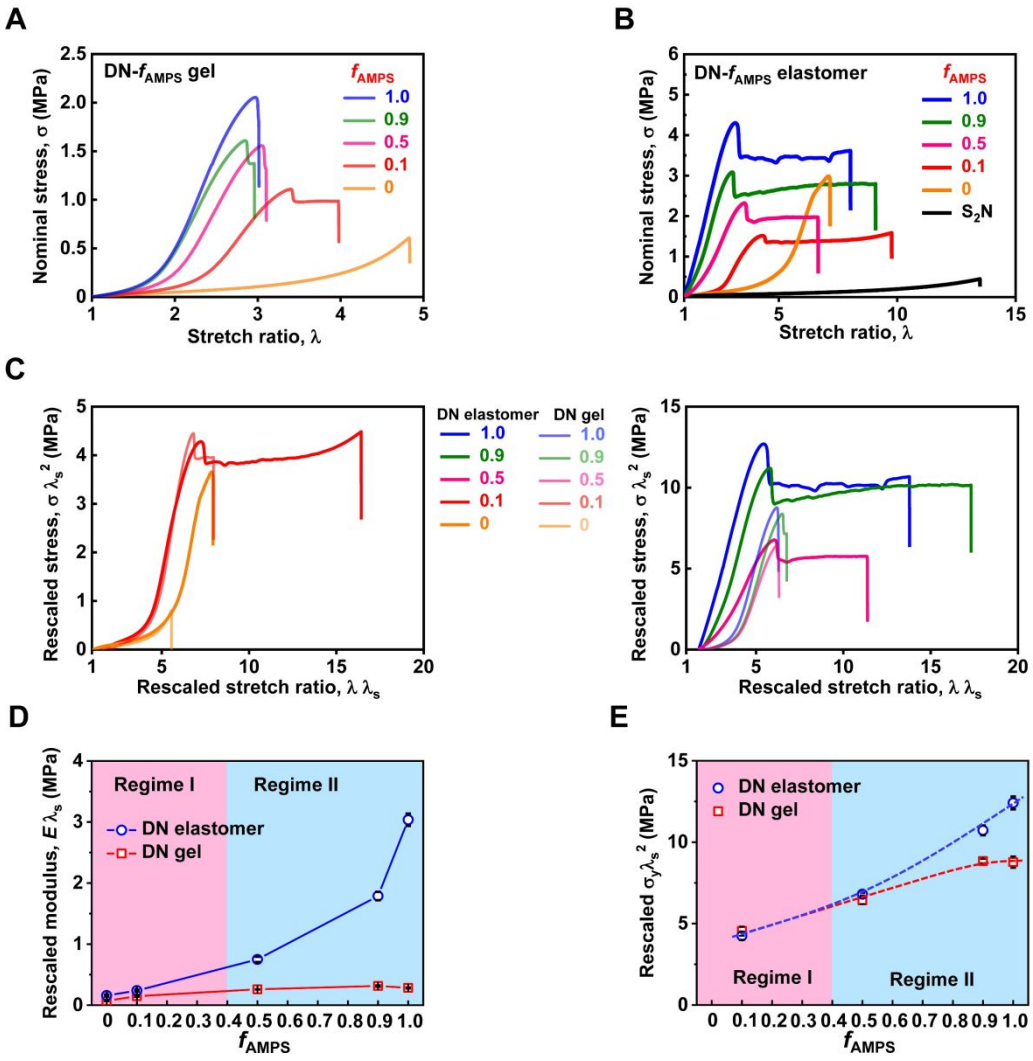

Figure 3. Uniaxial tensile behaviors of DN elastomers and DN gels. (A, B) Nominal stress (σ)–stretch-ratio (λ) curves for DN (A) gels and (B) elastomers prepared with various f_{AMPS} molar ratios. (C) Corresponding rescaled stress $\sigma\lambda_s^2$–rescaled stretch-ratio $\lambda\lambda_s$ curves for DN gels and elastomers. Left figure shows curves for f_{AMPS} = 0 and 0.1. Right figure shows curves for f_{AMPS} = 0.5, 0.9, and 1.0. (D) Rescaled modulus $E\lambda_s$ and (E) yielding stress $\sigma_y\lambda_s^2$ of DN gels and elastomers plotted as functions of f_{AMPS} molar ratio. In regimes I and II, DN elastomers are without and with obvious nanophase separation, respectively.

Energy-Dissipation Mechanism. As elucidated in previous studies, DN hydrogels are essentially toughened by mechanical-energy dissipation caused by the rupture of the first network strands, which is observed as mechanical hysteresis in cyclic tensile

and compressive tests[5]. In a chemically crosslinked elastic first network, an abundance of covalent bonds in the first network sacrificially ruptures upon deformation, thereby dissipating large amounts of energy[5, 11, 19]. Such chemical bond scission results in irreversible mechanical hysteresis. [5, 11, 31, 33, 35, 36] When the first network contains noncovalent crosslinks as dynamic sacrificial bonds, both reversible and irreversible mechanical hysteresis appear in cyclic tests.[8]

To clarify the energy-dissipation mechanism, we compared the continuous cyclic tensile behaviors of DN elastomers and the corresponding DN gels at various stretch ratios λ. For simplicity, the tests were performed without pausing between cycles. Figure 4A, B show the sequential loading-unloading curves of the DN-1.0 gel and DN-1.0 elastomer, respectively. Like conventional DN hydrogels[36], the DN-1.0 gel only exhibits irreversible hysteresis by the rupture of covalent bonds in the first network. For the DN-1.0 elastomer with strong phase separation, in addition to the irreversible hysteresis, a certain amount of reversible hysteresis is also observed. To compare the different efficiencies in energy dissipation in the DN elastomers and DN gels, we rescaled the loading-unloading curves using the same normalization method introduced in the previous section, and the results are shown in Figure 4C. For the same rescaled stretch ratio, the rescaled stress and energy dissipation of the DN-1.0 elastomer are significantly higher than those of the corresponding DN-1.0 gel. The rescaled accumulated irreversible energy dissipation (W_{irre}) and reversible hysteresis (W_{re}) of the DN-1.0 elastomers and gels estimated from the hysteresis-loop areas in Figure 4C are shown in Figure 4D and Figure 4E, respectively. The irreversible energy dissipation (W_{irre}) of the DN-1.0 elastomer is significantly higher than that of the DN-1.0 gel, and both increase with stretch ratio $\lambda_{max}\lambda_s$, where λ_{max} is the input maximum stretch ratio upon the loading. These results indicate that the strong phase-separated structure

considerably brings non-recoverable structure change upon stretching at the observation time scale. The reversible energy dissipation (W_{re}) of the DN-1.0 elastomer also show an increase with stretch ratio $\lambda_{max}\lambda_s$, while that of the DN-1.0 gel does not show W_{re}. The rescaled irreversible ratio (W_{irre}/W_{total}) of the DN-1.0 elastomer reaches ~80% at a high stretch ratio (Figure 4F), where W_{total} (= W_{irre}+ W_{re}) is the total work of extension applied to the samples.

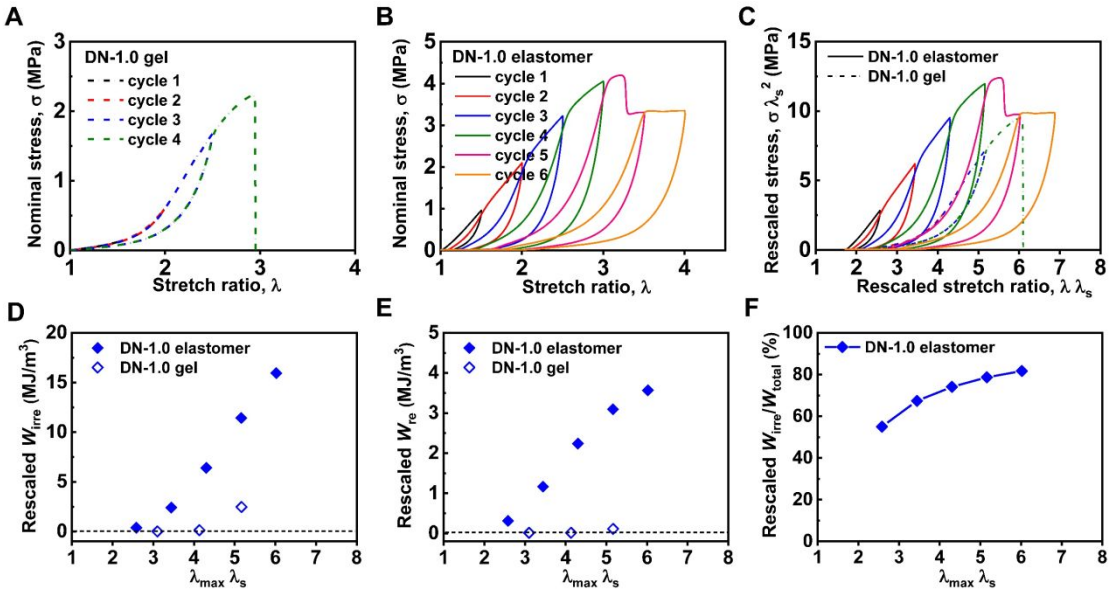

Figure 4. Comparison of rescaled energy-dissipation behaviors of phase-separated DN elastomer and DN gel. (A, B) Sequential loading–unloading cycles for DN-1.0 (A) gel and (B) elastomer. (C) Rescaled loading–unloading cycles for DN-1.0 gel and corresponding elastomer. (D–F) Rescaled (D) irreversible hysteresis (W_{irre}), (E) reversible hysteresis (W_{re}), and (F) irreversible fraction (W_{irre}/W_{total}) for DN-1.0 elastomer. For comparison, data for DN-1.0 gel are also shown in (D) and (E). The cyclic loading-unloading is performed with a strain rate of 0.14 s^{-1} and without waiting time between cycles.

While the reversible hysteresis could be attributed to the dynamic nature of dipole-dipole interaction in PAMPS-rich clusters, the irreversible energy dissipation could be originated from two different mechanisms. One is the cleavage of the covalent bonds of the first network in PAMPS-poor phase and the other is the plastic-like deformation of the PAMPS-rich phases. The collapsed PAMPS strands might be unfolded by breaking of the dipole-dipole interaction and the unfolded structure might be partially

frozen by reforming of the dipole-dipole interaction to show irreversible hysteresis in the cyclic tensile test. To clarify the different mechanisms of the irreversible energy dissipation, we characterize the covalent bond scission in the phase-separated DN-1.0 elastomer by comparing it with the corresponding DN-1.0 gel using an experimental protocol illustrated in Figure 5A. The virgin DN-1.0 elastomer samples were first stretched to different λ_{max} and then unloaded and immersed in NMF solvent to reach swollen equilibrium. The mechanical properties after swollen were tested. If significant bond scission occurs in DN-1.0 elastomer, the stretched and unloaded sample would show significant reduction in the mechanical behaviors after swollen in NMF compared with the corresponding DN-1.0 gel subjected to the same rescaled stretch ratio ($\lambda_{max}\lambda_s$) and swollen process. Figure 5B and 5C show that the rescaled tensile stress–stretch ratio curves overlap with each other for the pre-loaded ratio $\lambda_{max}\lambda_s \leq 4.0$, both for the swollen DN-1.0 elastomer and DN-1.0 gel. This indicates negligible internal fracture of the covalent bonds at small stretch for both materials. Further increasing loading to $\lambda_{max}\lambda_s \geq 6.0$, a significant reduction of the mechanical behaviors for both DN-1.0 elastomer and DN-1.0 gel is observed, indicating the rupture of first network covalent bond. As shown in Figure 5D, the rescaled modulus E_{swollen} (after swollen) decreases with the increase of $\lambda_{max}\lambda_s$, due to the enhanced "covalent sacrificial bond" scission at large deformation. Surprisingly, the E_{swollen} of DN-1.0 elastomer and DN-1.0 gel almost overlap at each rescaled stretch ratio $\lambda_{max}\lambda_s$, and the swelling degree of DN-1.0 elastomer and DN-1.0 gel is almost identical at the same $\lambda_{max}\lambda_s$ (Figure 5E), indicating that the covalent bond scission in DN-1.0 elastomer is almost the same as that in DN-1.0 gel at the same rescaled deformation, not influenced by the superimposing of the nanophase separation. This is reasonable considering that the dipole-dipole interaction is weaker than the covalent bonds and will break prior to the

covalent bonds. These results clearly indicate that the significantly enhanced irreversible hysteresis observed in DN-1.0 elastomer is not due to the chain scission but the plastic deformation of the PAMPS-rich phases. Such irreversible deformation of PAMPS-rich phases should depend on the observation time scale. We further studied the waiting time-dependence of the hysteresis reversibility of DN-1.0 elastomer at various λ_{max}. As shown in Figure 6, the reversible hysteresis shows very weak waiting-time dependence at all λ_{max}. Even for small λ_{max} of 2.5 and waiting for 12 h, the reversible hysteresis only increases slightly compared with the one with no waiting time. This result indicates that the lifetime of dipole-dipole interaction in non-polar media is relatively long at room temperature. We then investigated the thermal reversibility of DN-1.0 elastomers by heating the pre-loaded samples at 80 °C for 4 h. After the thermal treatment, the samples show significantly enhanced reversible hysteresis (Figure 6), suggesting that the unfolded PAMPS strands recover to their original collapsed state by thermal activation of the dipole-dipole interaction and the second-network mobility. It is worth noting that at small λ_{max} of 2.5 (corresponding to $\lambda_{max}\lambda_s \sim 4.0$), the recovered cycle after thermal treatment almost overlaps with the original cycle and the reversible hysteresis is recovered to 90 % (Figure 6A). This result also confirms that covalent bond scission hardly occurs at small deformation, which is consistent with the results in Figure 5. In contrast, for large λ_{max} of 4.0 and 5.5, where yielding significantly occurs, the reversible hysteresis of the cycles after thermal process are only recovered to 40 % of the original cycles, indicating that significant covalent bond scission occurs after yielding.

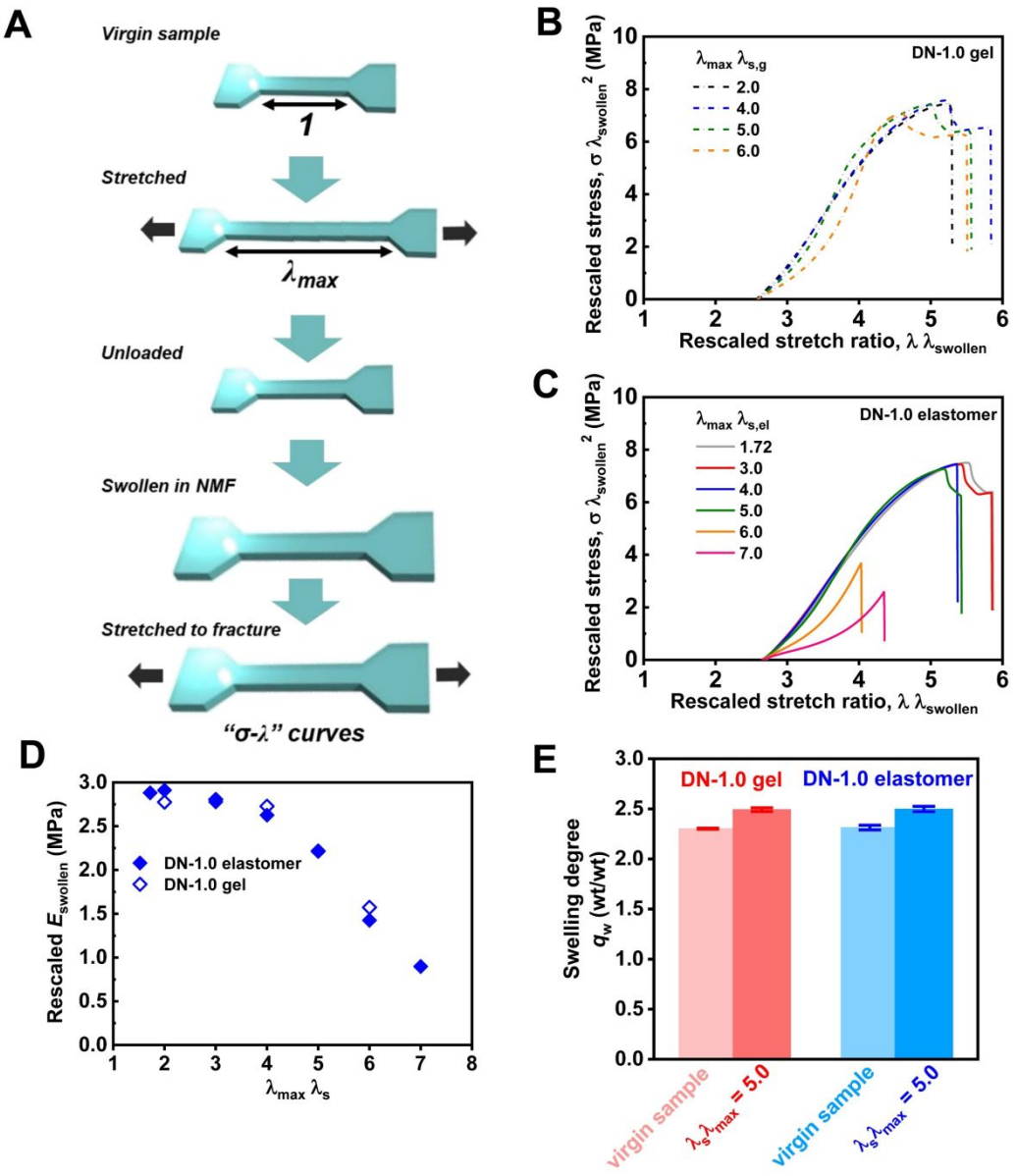

Figure 5. Comparison of rescaled mechanical properties of DN-1.0 elastomers and DN-1.0 gels subjected to preloading (λ_{max}) and swollen process. $\lambda_{swollen}$ denotes the pre-stretch ratio in the swollen state, which equals to the thickness ratio in relative to their corresponding as-synthesized S_1N gels. (A) Illustration for the experimental process. (B, C) Rescaled mechanical properties of DN-1.0 elastomer and DN-1.0 gel subjected to preloading and swollen process. (D) The rescaled modulus (after swollen) $E_{swollen}$ of DN-1.0 elastomers and DN-1.0 gels subjected to preloading and swollen process as a function of λ_{max} λ_s. (E) Swelling degree q_w of DN-1.0 elastomer and DN-1.0 gel in NMF solvent in virgin state and after stretching to $\lambda_{max}\lambda_s$ of 5.0. Swelling degree q_w is calculated from $q_w = (m_{swelling} - m_{dried})/m_{dried}$, where $m_{swelling}$ is sample weight after swelling in NMF and m_{dried} is the dried polymer weight.

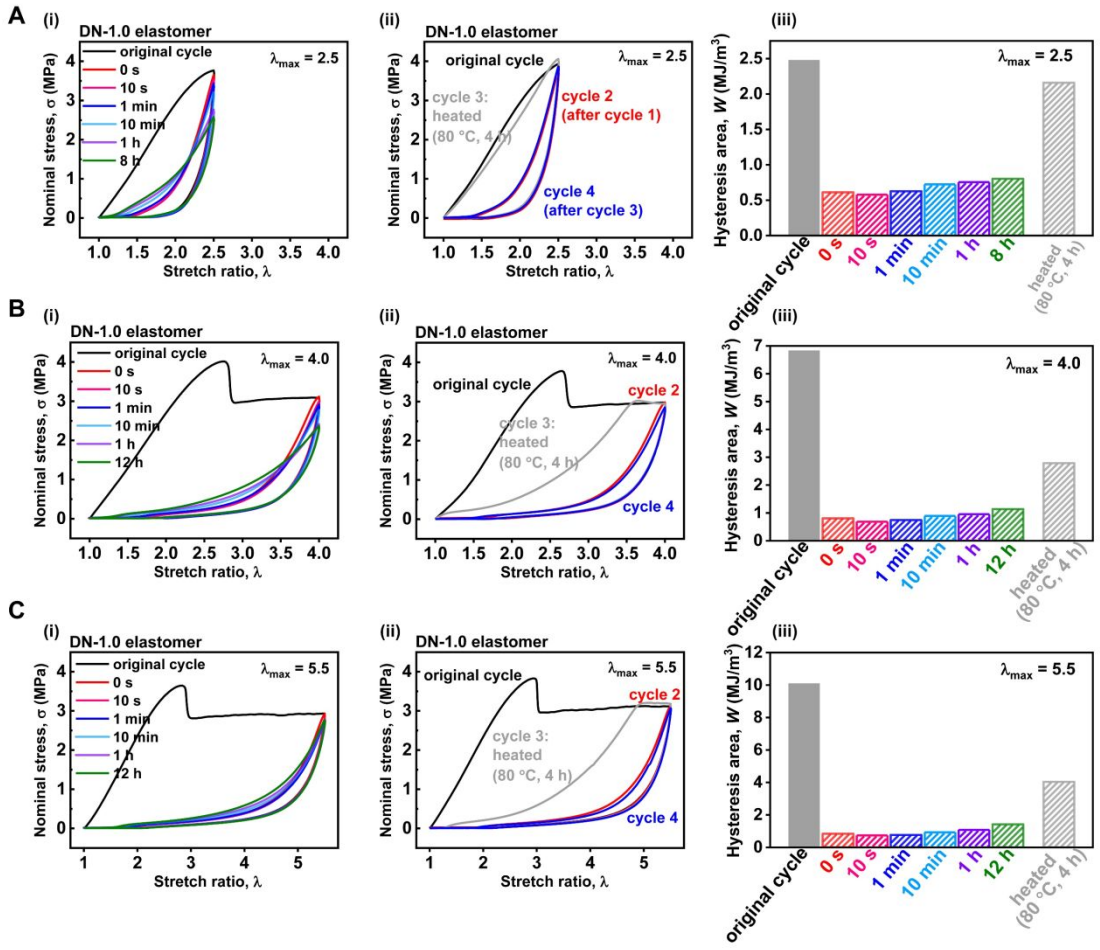

Figure 6. Weak waiting time-dependent reversibility and strong thermal reversibility of DN-1.0 elastomer. (A–C) Sequential loading–unloading curves (i, ii) and hysteresis area (iii) of DN-1.0 elastomer with different waiting times between the sequential cycles and after thermal process (heated at 80 °C for 4 h) for (A) λ_{max} = 2.5, (B) λ_{max} = 4.0 and (C) λ_{max} = 5.5. For (ii), the cycle 2 was conducted right after the original cycle without pausing, followed by the 4 h heating and the cycle 3; and the cycle 4 was conducted right after cycle 3 without pausing.

We further show the cyclic tensile tests of the DN gels and DN elastomers prepared for f_{AMPS} = 0.1, 0.5 in Figure S7 and S8 of the Supporting Information, respectively. For the DN-0.1 elastomer prepared without phase separation, the rescaled loading-unloading curves almost overlap with those of the DN-0.1 gel. As expected, the DN-0.1 elastomer shows fully irreversible mechanical hysteresis, like the DN-0.1 gel. These results indicate that the DN-0.1 elastomer without phase separation shows the same overall amount of covalent bond scission as the DN-0.1 gel. For the DN elastomers

with phase separation ($f_{AMPS} = 0.5$), the rescaled loading–unloading curves deviate from those of their corresponding DN gels. Overall, the deviation remarkably increases for increasing f_{AMPS}, implying the effect of phase-separated structure. Moreover, as shown in Figure 4E, Figure S7 and S8, all the DN-f_{AMPS} gels show negligible W_{re}. In contrast, the DN elastomers with $f_{AMPS} \geq 0.5$ exhibit large reversible hysteresis W_{re}, and the rescaled W_{re} considerably increases with increasing f_{AMPS}. All these results confirm that the phase-separated structure not only considerably enhances the irreversible energy dissipation by the plastic unfolding of collapsed PAMPS strands from the PAMPS-rich clusters but also dissipates reversible energy by breaking and reforming of dipole-dipole interaction in the PAMPS-rich phase.

Interestingly, although the amount of covalent bond scission in the phase-separated DN elastomers is almost the same as that in DN gels, the rescaled yielding stress of the phase-separated DN elastomers is much higher than that of the DN gels. Our previous study suggested that yielding corresponds to global first-network break into discontinuous fragments and the stress concentration heavily exists even in conventional DN gels.[37] In fact, only several % breakage of the first-network strands induces yielding for a typical DN hydrogel made with a PAMPS first network[36] and the actual yielding stress is only several percent of the theoretical value even for a DN gel made with a quite homogeneous Tetra-PEG first network[28]. As the covalent bond scission in DN-1.0 elastomer is not influenced by the superimposing of the nanophase separation, the much higher yielding stress of the DN elastomers than the corresponding DN gels suggests the stress concentration is somehow suppressed in the DN elastomers. The phase separation might significantly homogenize the tension of the overstressed PAMPS strands with different length in the PAMPS-poor phase.

Internal Fracture Mechanism. Taken together, all the results above suggest the

following deformation and internal fracture mechanisms for DN elastomers with and without phase-separated structure. For DN elastomers with no nanophase separation (such as DN-0.1), the internal fracture process of the first-network strands is the same as that of common DN hydrogels and multiple-network elastomers.[1, 11, 28, 33, 36, 38] Being modestly prestretched under loading, first-network strands can deform moderately by strand rearrangement. After reaching a certain deformation limit, the fully stretched strands are cleaved, showing fully irreversible hysteresis loss in cyclic tensile experiments. Upon further increased stretching, the first network breaks into discontinuous fragments by stress concentration, appearing as macroscopic yielding and necking. Such internal fracture mechanism increases the fracture energy at the crack tip to show high toughness in comparison with the single network materials.

For nanophase-separated DN elastomer (such as DN-1.0), nanophase separation further enhances the modulus, strength and energy dissipation of the material (Figure 7). The first-network strands in PAMPS-rich clusters (grey islands) are collapsed by dipole-dipole interaction and those in PAMPS-poor sea are highly stressed by contractile tension of the clusters. The phase separated structure not only causes overstressing of the first network strands to show remarkable increase in modulus, but also brings reversible and irreversible structural change even at very small deformations thereby dissipating large amount of energy. (i) At small deformation far below the yielding point ($\lambda << \lambda_y$), the collapsed PAMPS strands in the PAMPS-rich clusters are partially unfolded by breaking of the non-covalent dipole-dipole interactions in the stretching direction, causing significant energy dissipation, mostly irreversible at room temperature at the observation time-scale. (ii) At moderate deformation ($\lambda < \lambda_y$), along with further anisotropic unfolding of the PAMPS-rich clusters, the highly stressed PAMPS strands in PAMPS-poor phase start to irreversibly rupture by scission of

covalent bonds. (iii) At large deformation ($\lambda > \lambda_y$), the first network in PAMPS-poor phase ruptures globally, showing distinct yielding.

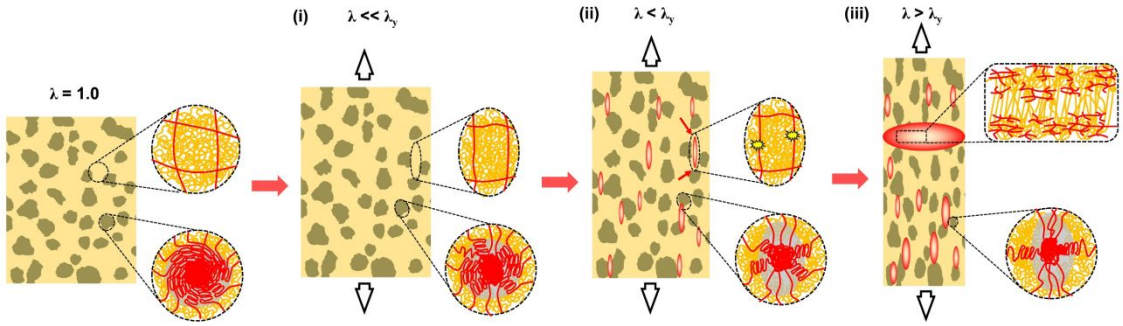

Figure 7. Proposed internal fracture mechanism of nanophase-separated DN elastomers during tensile deformation. The first-network strands in PAMPS-rich clusters (grey islands) are collapsed by dipole-dipole interaction and those in PAMPS-poor sea are highly stressed by contractile tension of the clusters. (i) At small deformation far below the yielding point ($\lambda << \lambda_y$), the collapsed PAMPS strands in the PAMPS-rich clusters are partially unfolded by breaking of the non-covalent dipole-dipole bonds in the stretching direction, causing significant energy dissipation, mostly irreversible at room temperature at the observation time-scale. (ii) At moderate deformation ($\lambda < \lambda_y$), along with further anisotropic unfolding of the PAMPS-rich clusters, the highly stressed PAMPS strands in PAMPS-poor phase start to irreversibly rupture by scission of covalent bonds. (iii) At large deformation ($\lambda > \lambda_y$), the first network in PAMPS-poor phase ruptures globally, showing distinct yielding. Formation of nanoclusters overstresses and homogenizes the tension of the sacrificial network, thereby remarkably increase the initial modulus and yielding stress; in the meanwhile, the nanoclusters might act as viscoelastic nanofillers dissipating energy and pinning the crack propagation, thereby significantly enhance toughness.

Toughness and Fatigue Resistance. The internal fracture mechanism by nanophase-separated structure is clearly elucidated in the above section. We next evaluate the toughness and fatigue resistance of nanophase-separated DN elastomer. To characterize the enhanced phase-separated-structure-induced toughness, tearing fracture tests were performed on trouser-shaped specimens (Figure 8A) to evaluate the fracture toughness of DN elastomers and DN gels as shown in Figure 8. Figure 8B and 8C present the normalized tearing force (force F divided by sample thickness h)-displacement curves as well as the tearing fracture energy T. The tearing forces and fracture energies of the DN elastomers were significantly enhanced compared with

those of the S_2N-matrix elastomer and the corresponding DN gels, and the properties became remarkably more enhanced with increasing f_{AMPS}. Especially, for DN-0.1 elastomer without phase-separation, the tearing fracture energy T is 2.0 kJ/m^2; while for strongly phase-separated DN-1.0 elastomer, the tearing fracture energy T is about 5 times enhanced as 10.8 kJ/m^2, suggesting the effect of the nanophase-separated structure on the fracture toughness.

Next, we evaluated the fatigue fracture properties of DN elastomers upon cyclic loading-unloading using prenotched samples in the pure shear geometry (Figure 8D), following the method by Suo and coworkers.[17, 18, 39] The DN-1.0 elastomer with phase separation and the DN-0.1 elastomer without phase separation were taken as examples. During cyclic loading, the maximum stretch ratio was kept constant at preset λ_{max}, and minimum stretch ratio was kept at 1.0. The extension of crack with cycles (c) was recorded, and plotted with cyclic number N (Figure S9). The crack propagation rate, dc/dN, was estimated from the slope of c versus N plot at steady state. The energy release rate G was obtained from stress-stretch ratio curve of unnotched sample when cyclic loading reaches steady state at the corresponding λ_{max} (Figure S10 and S11). Figure 8E and 8F show the dc/dN as a function of G. The results show the delayed fatigue crack propagation (slower dc/dN at the same G) and enhanced fatigue threshold of DN-1.0 elastomer compared to DN-0.1 elastomer. We obtained the fatigue threshold G_0 from the linear extrapolation of dc/dN ranging 60-600 nm/cycle in this work. For DN-0.1 elastomer without the phase-separated structure, the fatigue threshold G_0 is around 120 J/m^2, while for strongly phase-separated DN-1.0 elastomer, G_0 is about 5 times enhanced to be 615 J/m^2, which is consistent with the enhanced tearing fracture energy.

The fatigue threshold G_0 of elastomers is usually discussed using the Lake-Thomas

model as the energy required to break the covalent network across the crack interface in unit area.[17, 18, 39–41] However, our data should not be compared to the Lake-Thomas limit (~10^1 J/m^2 in typical) because the Lake-Thomas threshold is typically observed for the dc/dN in the order of ~10^0 nm/cycle[40, 41] while our G_0 was obtained from the dc/dN ranging 60-600 nm/cycle (Figure 8E). Note that such dc/dN range of ~100 nm/cycle is often characterized in fatigue experiments due to the feasibility on testing machine setup and experimental duration time.[17, 18, 39] Despite the difficulty to consider the molecular picture from the G_0 we obtained, much slower dc/dN as a function of G of the DN-1.0 elastomer than that of the DN-0.1elastomer is significant (Figure 8E and 8F), indicating enhanced fatigue durability by the phase-separated structure. The nanophase-separated structure in our DN elastomers should have some similarity with the nanocrystalline domains in anti-fatigue PVA gels reported by Zhao and coworkers[42, 43], showing that the hard phase could effectively pin fatigue cracks and greatly enhance the fatigue threshold of the materials (Figure 8G). A detailed mechanism of the phase-separated structure on the anti-fatigue properties should be studied in a separate work.

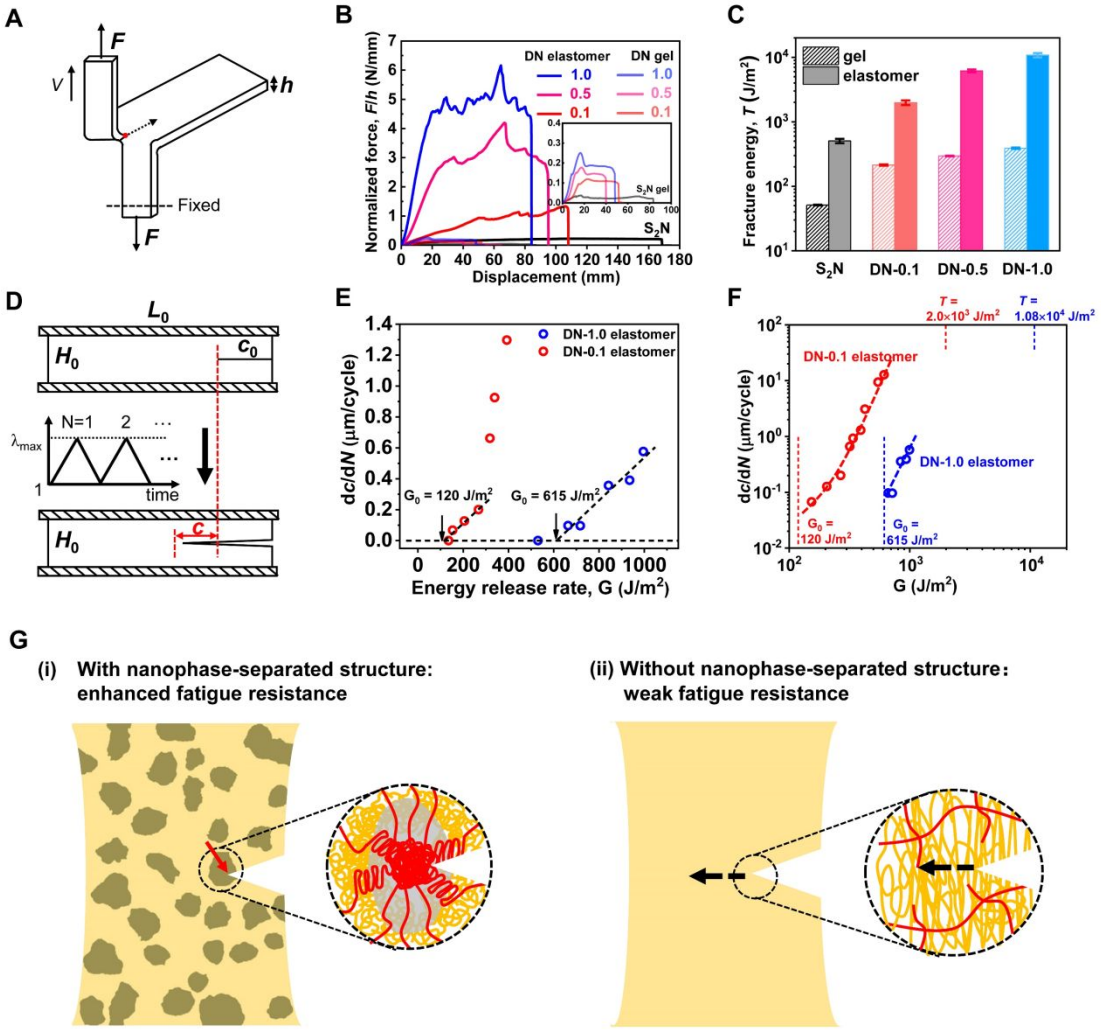

Figure 8. Significant enhancement in the tearing fracture resistance and fatigue resistance for phase-separated DN elastomers. (A) Experimental set-up for tearing test. (B) Force-displacement curves of tearing fractures and (C) corresponding fracture energies of DN elastomers and gels prepared with varied f_{AMPS} molar ratios. Inset of (B) shows enlarged tearing curves obtained for DN gels. For comparison, S_2N elastomer and gel of the second network are also shown in B and C. (D) Experimental set-up and geometry of the fatigue test (width L_0 = 50 mm, height H_0 =10 mm, initial notch length c_0 = 10 mm). (E) Crack propagation rate dc/dN as a function of the applied energy release rate G for DN-0.1 and DN-1.0 elastomers as examples. The fatigue threshold G_0 is obtained by linearly extrapolating the results to horizontal axis. (F) dc/dN versus the applied energy release rate G in logarithmic scale. For comparison, the tearing fracture energy of the two samples were indicated in the same plot. (G) Illustration of fatigue crack propagation in DN elastomers with and without nanophase-separated structure under cyclic loads.

CONCLUSION

In summary, by varying the ionic monomer fraction f_{AMPS} in the first-copolymer

network, we synthesized a series of DN elastomers with tunable nanophase-separated structures. Because the precursor DN gels with different f_{AMPS} have the same primary double-network structure, we could discuss the effect of f_{AMPS} on the nano-phase separation in the DN elastomers prepared by removal of cosolvent in the corresponding DN gels. We have clarified the multiple effects of the nanophase-separated structure on the mechanical properties of the DN elastomers: (1) the nanophase-separated structure highly stresses and homogenizes the tension of the first-network strands in the PAMPS-poor sea, thereby enhancing the elastic modulus and yielding stress; (2) the PAMPS-rich phases could act as viscoelastic nanofillers, dissipating large amount of energy, both irreversible and reversible, and suppressing the macroscopic crack propagation, thereby enhancing the toughness and fatigue resistance. The interplay mechanism between the double network effect and nanophase-separation effect clarified in this work shows that superimposing high-order structures in double network materials could bring further strengthening and toughening of the materials. Such strategy should be a universal approach for elastomers and gels in principle, which opens broad research opportunities, and will facilitate more researches as the next stage of the strengthening and toughening of the soft materials.

MATERIALS AND METHODS

Sample Synthesis

Materials. 2-Acrylamido-2-methylpropanesulfonic acid (AMPS; Toagosei Co., Ltd.) and 2-methoxyethyl acrylate (MEA; Fujifilm Wako Pure Chemical Corporation, Ltd.), as monomer, were used as received. *N*-methyl formamide (NMF; Fujifilm Wako Pure Chemical Corporation, Ltd.), as solvent, was used as received. Poly(ethylene glycol) diacrylate (PEGDA, average M_n 250; Sigma-Aldrich Co., LLC.), as crosslinker, was used as received. Benzophenone (BP; KANTO Chemical Co., Inc.), as radical initiator,

was used as received.

Synthesis of P(MEA-co-AMPS) Copolymer gels as First Network. An organic solution of C_m (M) monomer, x_1 (mol %) PEGDA as cross-linker, y_1 (mol %) BP as radical initiator and NMF as solvent was prepared. The concentrations (mol %) of the cross-linker and the initiator are in relative to the total monomer concentration C_m. For the monomer, non-polar monomer MEA and electrolyte monomer AMPS were mixed at various monomer fraction f_{AMPS} with the same overall monomer concentration C_m (M). To synthesize P(MEA-*co*-AMPS) gels, the overall monomer concentration, monomer fraction of AMPS, cross-linker concentration and initiator concentration were C_m = 1.8 M, f_{AMPS} = 0–1.0, x_1= 4 mol % and y_1 = 1 mol %, respectively. The precursor solutions were moved to an argon glovebox and were poured into glass plate molds separated by 1.0 mm thick silicone rubber spacers. We irradiated the polymerization with UV light (365 nm, 4 mW cm^{-2}) for 8 h to synthesize the first network. The as prepared P(MEA-*co*-AMPS) copolymer gels were referred to as S_1N-f_{AMPS}.

Synthesis of DN Elastomers and S_2N Elastomers. For the synthesis of P(MEA-*co*-AMPS)/PMEA DN elastomers, the as synthesized P(MEA-*co*-AMPS) S_1N gels with various f_{AMPS} were immersed in the second precursor solution for 1 day to reach equilibrium swelling state. The second precursor solution comprises MEA (60 wt %, that is, 4.7 M), 0.2 mol % PEGDA as cross-linker, 0.2 mol % BP as radical initiator and NMF as solvent. Each of the P(MEA-*co*-AMPS) S_1N gel swollen in the second precursor solution was sandwiched between two flat soda lime glass plates. Then, it was moved to the argon glovebox. The polymerization was irradiated with UV light (365 nm, 4 mW cm^{-2}) for 9 h to synthesize the PMEA second network (referred to as

S_2N network) in the presence of the P(MEA-*co*-AMPS) S_1N network. The synthesized DN-f_{AMPS} gels were then stored in vacuum oven at 80 °C for 24 h to completely remove the solvent to obtain DN-f_{AMPS} elastomers. For reference, the S_2N gels were also synthesized from the second precursor solution and were stored in vacuum oven at 80 °C for 24 h to obtain S_2N elastomers. Linear swelling ratio λ_s was determined by the sample thickness divided by the thickness of silicone rubber spacer (=1.0 mm) in the first step synthesis.

Structure Analysis

Static Small Angle X-Ray Scattering Measurement. The static SAXS measurement for DN elastomers and DN gels with varied f_{AMPS} from 0 to 1.0 was conducted in BL19U2 beamline of the National Center for Protein Sciences Shanghai at the Shanghai Synchrotron Radiation Facility, China. The X-ray energy, the wavelength of X-ray and the sample-to-detector distance were 12 keV, 0.9184 Å and 5934.0 mm, respectively. A Pilatus 1 M detector with a resolution of 981 × 1043 pixels and pixel size of 172 μm was used to record 2D SAXS patterns. All the SAXS data was analyzed with Fit 2D software from European Synchrotron Radiation Facility.

Transmission Electron Microscopy Observation. The DN-1.0 elastomer sample was immersed in 0.1 M CsCl aqueous solution for 24h to replace counter ion H^+ of PAMPS with Cs^+ ion. The sample was then dried in vacuum oven at 80 °C for 12 h to obtain Cs^+ stained DN elastomer sample. The cross-section of the Cs^+ stained DN elastomer with thickness of 200 nm were cut at −100 °C using an ultra-microtome (EM UC7i, Leica Microsystems, Germany) and then placed on a copper mesh grid. The transmission electron microscopy (TEM) observation was conducted using a Hitachi

H-7650 transmission electron microscope. The acceleration voltage of the electron gun for observation was 100 kV.

Mechanical Measurement

Tensile Test. Tensile mechanical properties of the gels and elastomers were measured with a commercial mechanical test machine (INSTRON 5965, Instron Co.) in air. The testing samples were cut into a dumbbell shape standardized as JISK6251-7 size (gauge length 12 mm, width 2 mm) with a gel cutting machine (Dumbbell Co., Ltd.). All the DN elastomers were tested immediately after solvent removal in vacuum oven at 80 °C for 24 h. The nominal stress (σ)-stretch ratio (λ) curves were recorded while the samples were stretched at a constant velocity of 100 mm/min (strain rate of 0.14 s^{-1}). The Young's modulus, E, was determined as the slope of σ-λ curves between the λ range of 1.02–1.1. The yielding stretch ratio and stress, λ_y and σ_y, were determined at the zero-slope point of the σ-λ curves. Each data point was the average of 3 measurements, and the error bars represented their standard deviations.

Cyclic Tensile Test. Cyclic tensile tests were performed using the same experimental setup of tensile tests. The samples were stretched to a pre-set stretch ratio, followed by unloading at the same strain rate, and the sequential loading-unloading cycles with increased stretch ratios were performed without waiting time. For the rescaling of energy dissipation behaviors of DN gels and DN elastomers, we rescaled the nominal stress σ and stretch ratio λ as $\sigma\lambda_s^2$ and $\lambda\lambda_s$, respectively, where λ_s is $\lambda_{s,\,g}$ and $\lambda_{s,\,el}$ for DN gels and DN elastomers. The rescaled irreversible energy dissipation, W_{irre}, was calculated from the sequential loading curves of the original stress (σ) – elongation ratio (λ) data. For a maximum stretch ratio (λ_{max_n}) of the n^{th} cycle, the

rescaled irreversible energy dissipation $W_{\text{irre\_}n}$ is calculated as the total accumulated irreversible part of dissipated energy of the original σ–λ curves multiplied by a prefactor ($\lambda_s{}^3$):

$$W_{\text{irre\_}n} = \lambda_s{}^3 \sum_{i=1}^{n} \left(\int_1^{\lambda_{\max\_n}} \sigma_{\text{load\_}n}\, d\lambda \; - \; \int_1^{\lambda_{\max\_n}} \sigma_{\text{load\_}n+1}\, d\lambda \right)$$

where $\sigma_{\text{load\_}n}$ is the stress of the n^{th} loading curve. The prefactor $\lambda_s{}^3$ is the rescaling factor because the rescaled stress and elongation ratio are $\sigma\lambda_s{}^2$ and $\lambda\lambda_s$, respectively. The rescaled reversible energy dissipation, W_{re}, was calculated from the sequential loading curves of the original σ– λ data. For a maximum stretch ratio ($\lambda_{\max\_n}$) of the n^{th} cycle, the rescaled reversible energy dissipation $W_{\text{re\_}n}$ is calculated as the irreversible part of dissipated energy of the original σ–λ curves multiplied by the prefactor ($\lambda_s{}^3$):

$$W_{\text{re\_}n} = \lambda_s{}^3 \left(\int_1^{\lambda_{\max\_n}} \sigma_{\text{load\_}n+1}\, d\lambda \; - \; \int_1^{\lambda_{\max\_n}} \sigma_{\text{unload\_}n}\, d\lambda \right)$$

where $\sigma_{\text{unload\_}n}$ is the stress of the n^{th} unloading curve.

The rescaled total energy dissipation, W_{total}, is given as:

$W_{\text{total\_}n} = W_{\text{irre\_}n} + W_{\text{re\_}n}$.

Tearing Fracture Test. The tearing fracture tests were performed with a commercial mechanical test machine (INSTRON 5965, Instron Co.) in air. The testing samples were cut into the trouser shape geometry, which has the standardized JIS-K6252 1/ 2 size (width $2b_0$ = 7.5 mm, length a_0 = 50 mm, the length of the initial notch is 20 mm), with a gel cutting machine (Dumbbell Co., Ltd.). The two arms of the test sample were clamped, and the one was pulled upward at a velocity of 100 mm/min, while the other was maintained stationary. The tearing force F was recorded. The tearing fracture

energy T is calculated from the average value of F at steady state during tearing and the sample thickness h according to the relation $T = \frac{2F}{h}$.

Fatigue Experiment. Cyclic fatigue experiments were performed on a tensile tester (Shimadzu Autograph AG-X tensile machine) with a 1000 N load cell. Sample with pure shear geometry (10×50×1.70 mm^3, $H_0 \times L_0 \times t$) was used. To track the crack propagation with cyclic loading, an initial crack with length 10 mm along L_0 was cut (Figure 8D). Cyclic loading was performed along the H_0 direction. The maximum elongation ratio in each cycle was held at λ_{max}, while the minimum was held at λ=1.0. The nominal strain rate was kept at 1.0 s^{-1}. The test temperature and room humidity were kept constant at 24 ℃ and 25%, respectively. We used a digital camera (Canon EOS Kiss X5) to record photos during crack extension for the notched samples every 2 min. The length of crack extension under cyclic loading was recorded as c. The energy release rate G was estimated by $G = W_e(\lambda_{max}) \times H_0$, where H_0 is the initial sample height, and $W_e(\lambda_{max})$ is the elastic strain energy density of the unnotched sample at steady state under the corresponding λ_{max} (Figure S10 and S11). Since softening and shakedown occurred during cyclic loading, the $W_e(\lambda_{max})$ was calculated from the integral area under the unloading curve at the 5000th cycle where the stress-stretch ratio curves reached the steady state.

ASSOCIATED CONTENT

Supporting Information. A table showing the summarized mechanical properties of

DN elastomers and gels; swelling comparison of S_1N prepared with and without electrolyte component in second monomer solution; SAXS results of DN gels; domain spacing d_0 and $FWHM/q_{peak}$ of DN elastomers plotted as functions of f_{AMPS} molar fraction; reswelling of DN-1.0 elastomer in NMF; DSC thermograms of DN elastomers; rescaled yielding stretch ratio $\lambda_y\lambda_s$ of DN gels and elastomers plotted as functions of f_{AMPS}; comparison of rescaled energy-dissipation behaviors of DN-0.1 elastomer and corresponding gel; comparison of rescaled energy-dissipation behaviors of DN-0.5 elastomer and corresponding gel; crack propagation length *c* as a function of the number of cycles *N* with different applied stretch ratio λ_{max} for DN-1.0 and DN-0.1 elastomers; experimental set-up and characterizing the energy release rate *G* for DN-1.0 elastomer and DN-0.1 elastomer.

ACKNOWLEDGMENTS

This research was supported by the Japan Society for the Promotion of Science (JSPS) KAKENHI (grant nos. JP17H06144, JP17H04891, and JP19K23617). The Institute for Chemical Reaction Design and Discovery (ICReDD) was established by World Premier International Research Initiative (WPI), MEXT, Japan. The authors gratefully acknowledge staffs from BL19U2 beamline of the National Facility for Protein Science in Shanghai (NFPS) at the Shanghai Synchrotron Radiation Facility for their assistance during data collection. Y. Z. thanks the China Scholarship Council (CSC) for financial support during his Ph.D. studies.

CONFLICTS OF INTEREST

The authors declare no conflicts of interest.

REFERENCES

(1) Creton, C. 50th anniversary perspective: Networks and gels: soft but dynamic and tough. *Macromolecules* **2017**, 50 (21), 8297-8316.

(2) Roland, C. Unconventional rubber networks: Circumventing the compromise between stiffness and strength. *Rubber Chemistry and Technology* **2013**, 86 (3), 351-366.

(3) Ansarifar, A.; Chen, Y.; Job, A. E.; Hashim, A. S.; Heinrich, G.; Riyajan, S.-A.; Thakore, S. I.; Mou'ad, A. T.; Abd-El-Aziz, A. S.; Craig, S., *Natural Rubber Materials: Volume 2: Composites and Nanocomposites*. Royal Society of Chemistry: 2013; p 26-27.

(4) Nakajima, T. Generalization of the sacrificial bond principle for gel and elastomer toughening. *Polym. J.* **2017**, 49 (6), 477-485.

(5) Gong, J. P. Why are double network hydrogels so tough? *Soft Matter* **2010**, 6 (12), 2583-2590.

(6) Gong, J. P.; Katsuyama, Y.; Kurokawa, T.; Osada, Y. Double-network hydrogels with extremely high mechanical strength. *Adv. Mater.* **2003**, 15 (14), 1155-1158.

(7) Chen, Q.; Zhu, L.; Zhao, C.; Wang, Q.; Zheng, J. A robust, one-pot synthesis of highly mechanical and recoverable double network hydrogels using thermoreversible sol-gel polysaccharide. *Adv. Mater.* **2013**, 25 (30), 4171-4176.

(8) Sun, J.-Y.; Zhao, X.; Illeperuma, W. R.; Chaudhuri, O.; Oh, K. H.; Mooney, D. J.; Vlassak, J. J.; Suo, Z. Highly stretchable and tough hydrogels. *Nature* **2012**, 489 (7414), 133-136.

(9) Zhang, H. J.; Sun, T. L.; Zhang, A. K.; Ikura, Y.; Nakajima, T.; Nonoyama, T.; Kurokawa, T.; Ito, O.; Ishitobi, H.; Gong, J. P. Tough physical double-network hydrogels based on amphiphilic triblock copolymers. *Adv. Mater.* **2016**, 28 (24), 4884-4890.

(10) Kamio, E.; Yasui, T.; Iida, Y.; Gong, J. P.; Matsuyama, H. Inorganic/organic double-network gels containing ionic liquids. *Adv. Mater.* **2017**, 29 (47), 1704118.

(11) Ducrot, E.; Chen, Y.; Bulters, M.; Sijbesma, R. P.; Creton, C. Toughening elastomers with sacrificial bonds and watching them break. *Science* **2014**, 344 (6180), 186-189.

(12) Sun, T. L.; Kurokawa, T.; Kuroda, S.; Ihsan, A. B.; Akasaki, T.; Sato, K.; Haque, M. A.; Nakajima, T.; Gong, J. P. Physical hydrogels composed of polyampholytes demonstrate high toughness and viscoelasticity. *Nat. Mater.* **2013**, 12 (10), 932-937.

(13) Mayumi, K.; Guo, J.; Narita, T.; Hui, C. Y.; Creton, C. Fracture of dual crosslink gels with permanent and transient crosslinks. *Extreme Mech. Lett.* **2016**, 6, 52-59.

(14) Rose, S. v.; Dizeux, A.; Narita, T.; Hourdet, D.; Marcellan, A. Time dependence of dissipative and recovery processes in nanohybrid hydrogels. *Macromolecules* **2013**, 46 (10), 4095-4104.

(15) Dai, X.; Zhang, Y.; Gao, L.; Bai, T.; Wang, W.; Cui, Y.; Liu, W. A Mechanically strong, highly stable, thermoplastic, and self-healable supramolecular polymer hydrogel. *Adv. Mater.* **2015**, 27 (23), 3566-3571.

(16) Yang, C. H.; Wang, M. X.; Haider, H.; Yang, J. H.; Sun, J.-Y.; Chen, Y. M.; Zhou, J.; Suo, Z. Strengthening alginate/polyacrylamide hydrogels using various multivalent cations. *ACS Appl. Mater. Interfaces* **2013**, 5 (21), 10418-10422.

(17) Zhang, W.; Hu, J.; Tang, J.; Wang, Z.; Wang, J.; Lu, T.; Suo, Z. Fracture toughness and fatigue threshold of tough hydrogels. *ACS Macro Lett.* **2018**, 8 (1), 17-23.

(18) Zhang, W.; Liu, X.; Wang, J.; Tang, J.; Hu, J.; Lu, T.; Suo, Z. Fatigue of double-network hydrogels. *Eng. Fract. Mech.* **2018**, 187, 74-93.

(19) Matsuda, T.; Nakajima, T.; Gong, J. P. Fabrication of tough and stretchable hybrid double-network elastomers using ionic dissociation of polyelectrolyte in nonaqueous media. *Chem. Mater.* **2019**, 31 (10), 3766-3776.

(20) Kusoglu, A.; Weber, A. Z. New insights into perfluorinated sulfonic-acid ionomers. *Chem. Rev.* **2017**, 117 (3), 987-1104.

(21) Wang, C.; Wiener, C. G.; Fukuto, M.; Li, R.; Yager, K. G.; Weiss, R.; Vogt, B. D. Strain rate dependent nanostructure of hydrogels with reversible hydrophobic associations during uniaxial extension. *Soft Matter* **2019**, 15 (2), 227-236.

(22) Chen, D. Y.; Hickner, M. A. Ion clustering in quaternary ammonium functionalized benzylmethyl containing poly(arylene ether ketone)s. *Macromolecules* **2013**, 46 (23), 9270-9278.

(23) Disabb-Miller, M. L.; Johnson, Z. D.; Hickner, M. A. Ion motion in anion and proton-conducting triblock copolymers. *Macromolecules* **2013**, 46 (3), 949-956.

(24) Chen, C.; Pan, J.; Han, J. J.; Wang, Y.; Zhu, L.; Hickner, M. A.; Zhuang, L. Varying the microphase separation patterns of alkaline polymer electrolytes. *J. Mater. Chem. A* **2016**, 4 (11), 4071-4081.

(25) Tsujita, Y.; Yasuda, M.; Takei, M.; Kinoshita, T.; Takizawa, A.; Yoshimizu, H. Structure of Ionic Aggregates of Ionomers. 1. Variation in the Structure of Ionic Aggregates with Different Acid Content and Degree of Neutralization of Ethylene and Styrene Ionomers. *Macromolecules* **2001**, 34 (7), 2220-2224.

(26) Rubinstein, M.; Colby, R. H., *Polymer physics*. Oxford university press New York: **2003**; Vol. 23; p 259.

(27) Guo, H.; Uehara, Y.; Matsuda, T.; Kiyama, R.; Li, L.; Ahmed, J.; Katsuyama, Y.; Nonoyama, T.; Kurokawa, T. Surface charge dominated protein absorption on

hydrogels. *Soft Matter* **2020**, 16 (7), 1897-1907.

(28) Matsuda, T.; Nakajima, T.; Fukuda, Y.; Hong, W.; Sakai, T.; Kurokawa, T.; Chung, U.-i.; Gong, J. P. Yielding criteria of double network hydrogels. *Macromolecules* **2016**, 49 (5), 1865-1872.

(29) Nakajima, T.; Ozaki, Y.; Namba, R.; Ota, K.; Maida, Y.; Matsuda, T.; Kurokawa, T.; Gong, J. P. Tough double-network gels and elastomers from the nonprestretched first network. *ACS Macro Lett.* **2019**, 8 (11), 1407-1412.

(30) Chen, Q.; Tudryn, G. J.; Colby, R. H. Ionomer dynamics and the sticky rouse model. *J. Rheol.* **2013**, 57 (5), 1441-1462.

(31) Na, Y. H.; Tanaka, Y.; Kawauchi, Y.; Furukawa, H.; Sumiyoshi, T.; Gong, J. P.; Osada, Y. Necking phenomenon of double-network gels. *Macromolecules* **2006**, 39 (14), 4641-4645.

(32) Tirumala, V. R.; Tominaga, T.; Lee, S.; Butler, P. D.; Lin, E. K.; Gong, J. P.; Wu, W.-l. Molecular model for toughening in double-network hydrogels. *J. Phys. Chem. B.* **2008**, 112 (27), 8024-8031.

(33) Millereau, P.; Ducrot, E.; Clough, J. M.; Wiseman, M. E.; Brown, H. R.; Sijbesma, R. P.; Creton, C. Mechanics of elastomeric molecular composites. *Proc. Natl. Acad. Sci.* **2018**, 115 (37), 9110-9115.

(34) Ducrot, E.; Creton, C. Characterizing large strain elasticity of brittle elastomeric networks by embedding them in a soft extensible matrix. *Adv. Funct. Mater.* **2016**, 26 (15), 2482-2492.

(35) Webber, R. E.; Creton, C.; Brown, H. R.; Gong, J. P. Large strain hysteresis and mullins effect of tough double-network hydrogels. *Macromolecules* **2007**, 40 (8), 2919-2927.

(36) Nakajima, T.; Kurokawa, T.; Ahmed, S.; Wu, W.-l.; Gong, J. P. Characterization of internal fracture process of double network hydrogels under uniaxial elongation. *Soft Matter* **2013**, 9 (6), 1955-1966.

(37) Fukao, K.; Nakajima, T.; Nonoyama, T.; Kurokawa, T.; Kawai, T.; Gong, J. P. Effect of relative strength of two networks on the internal fracture process of double network hydrogels as revealed by in situ small-angle X-ray scattering. *Macromolecules* **2020**, 53 (4), 1154-1163.

(38) Ducrot, E.; Montes, H.; Creton, C. Structure of tough multiple network elastomers by small angle neutron scattering. *Macromolecules* **2015**, 48 (21), 7945-7952.

(39) Tang, J.; Li, J.; Vlassak, J. J.; Suo, Z. Fatigue fracture of hydrogels. *Extreme Mech. Lett.* **2017,** 10, 24-31.

(40) Lake, G.; Thomas, A. The strength of highly elastic materials. *Proc. R. Soc. London A.* **1967,** 300 (1460), 108-119.

(41) Lake, G. Aspects of fatigue and fracture of rubber. *Progress of Rubber Technology* **1983**, 45, 89-143.

(42) Lin, S.; Liu, X.; Liu, J.; Yuk, H.; Loh, H.-C.; Parada, G. A.; Settens, C.; Song, J.; Masic, A.; McKinley, G. H. Anti-fatigue-fracture hydrogels. *Sci. Adv.* **2019***,* 5 (1), eaau8528.
(43) Lin, S.; Liu, J.; Liu, X.; Zhao, X. Muscle-like fatigue-resistant hydrogels by mechanical training. *Proc. Natl. Acad. Sci.* **2019,** 116 (21), 10244-10249.

TOC Graphic

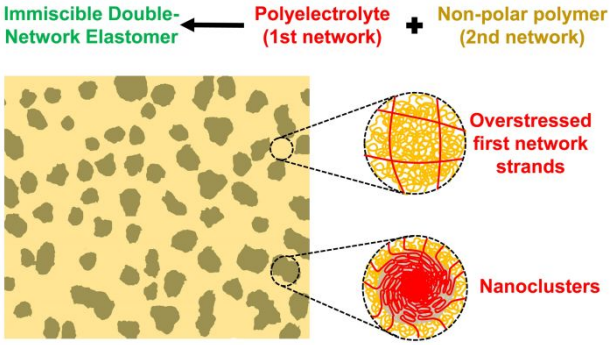
Immiscible Double-Network Elastomer
Polyelectrolyte (1st network)
Non-polar polymer (2nd network)
Overstressed first network strands
Nanoclusters